Open Archive Toulouse Archive Ouverte (OATAO)

OATAO is an open access repository that collects the work of Toulouse researchers and makes it freely available over the web where possible

This is an author's version published in: http://oatao.univ-toulouse.fr/27428

Official URL: https://doi.org/10.1088/1361-6528/ab494f

Any correspondence concerning this service should be sent to the repository administrator: tech-oatao@listes-diff.inp-toulouse.fr

Near-infrared/visible-emitting nanosilica modified with silylated Ru(II) and Ln(III) complexes

Rafael Miguel Sábio[1,2] ⓘ **, Silvia Helena Santagneli**[1]**, Marie Gressier**[2]**,**
José Maurício Almeida Caiut[3]**, Wallance Moreira Pazin**[4]**,**
Sidney José Lima Ribeiro[1] **and Marie-Joëlle Menu**[2]

[1] Institute of Chemistry, São Paulo State University, UNESP, CP355 Araraquara SP, Brazil
[2] CIRIMAT Université de Toulouse, CNRS, INPT, UPS, Toulouse, France. 118 route de Narbonne, F 31062 Toulouse Cedex 9, France
[3] Departamento de Química, Faculdade de Filosofia, Ciências e Letras de Ribeirão Preto, Universidade de São Paulo, 14040 901 Ribeirão Preto, SP, Brazil
[4] Departamento de Física, Faculdade de Filosofia, Ciências e Letras de Ribeirão Preto, Universidade de São Paulo, 14040 901 Ribeirão Preto, SP, Brazil

E mail: rafaelmsabio@gmail.com

Abstract
Three luminescent silica-based nanohybrids were fabricated by grafting of silylated Ru(II) and Nd/Yb(III) complexes onto mesoporous silica nanoparticles obtained by microemulsion method. The prepared nanohybrids were characterized by Fourier transform-Raman spectroscopy, solid state-nuclear magnetic resonance, high resolution-transmission electron microscopy and scanning and transmission electron microscopy techniques. The chemical integrity and the grafting of all complexes inside MSNs nanopores as well as a good distribution of metal complexes onto MSNs surface were achieved for all nanohybrids. Photophysical results revealed that by monitoring the excitation on Ru(II) moieties from **SiO$_2$–RuNd** and **SiO$_2$–RuYb** nanohybrids, the sensitization of NIR-emitting Nd/Yb(III) ions were successfully detected via energy transfer processes. Energy transfer rates (k_{EnT}) of 0.20×10^7 and 0.11×10^7 s^1 and efficiencies of energy transfer (η_{EnT}) of 40% and 27.5% were obtained for **SiO$_2$–RuNd** and **SiO$_2$–RuYb** nanohybrids, respectively. These results confirm the preparation of promising dual (near-infrared/visible)-emitting silica-based nanohybrids as new nanotools for applications as nanosensores and nanomarkers.

Supplementary material for this article is available online

Keywords: silylated Ru(II) and Ln(III) complexes, mesoporous silica nanoparticles, dual-emitting silica-based nanohybrids

(Some figures may appear in colour only in the online journal)

1. Introduction

Lanthanide complexes have been extensively studied due their fascinating optical properties usually governed by interaction with light. By using organic chromophores as coordinating agents, the excitation process could be improved and the emission of lanthanide centers will be intensified [1, 2]. Intense and narrow emission bands, high quantum yields and long emission lifetimes could be achieved been suitable for industrial applications such as optical fibers, amplifiers, displays and lasers [3, 4] as well as biological applications including *in vitro* and *in vivo* biomarkers [5, 6], biosensors [7], magnetic ressonance contrasts (MRI) [8], photothermal and photodynamic therapies (PTT and PDT)
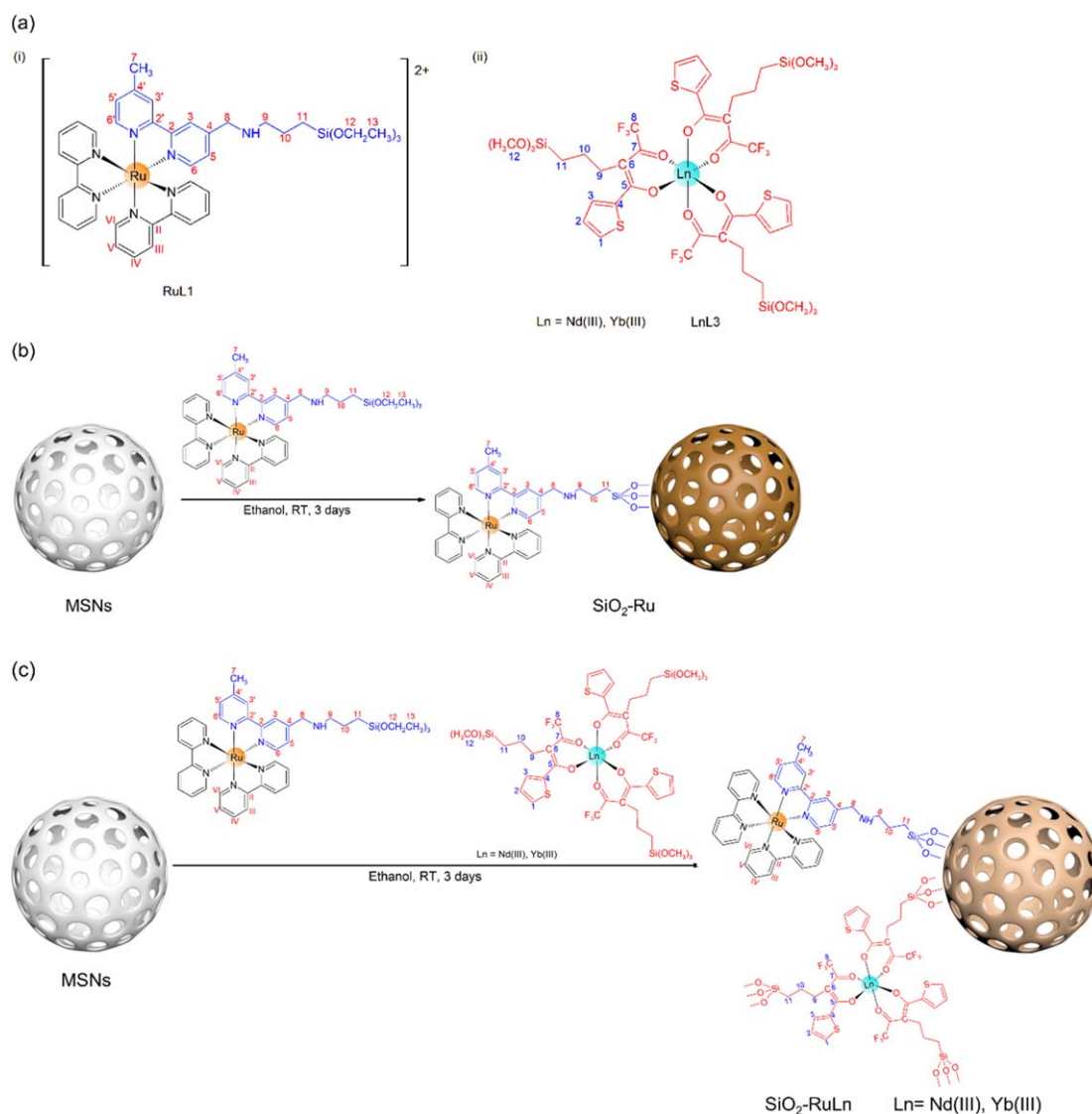
Scheme 1. RuL1 (a, i) and **LnL3** (a, ii) complexes and synthesis routes to fabricate **SiO₂ Ru** (b) and **SiO₂ RuLn** (c) nanohybrids (described the numbers in red and blue).

[9, 10] and so forth. Specifically, near-infrared emitting lanthanide(III) complexes such as Nd(III) and Yb(III) have been garnered great attention due to their emission bands ranging from 700 to 1100 nm, spectral domain of high transparency in biological systems extremely interesting for biomedical applications [4, 11]. However, antenna ligands are commonly excited by ultraviolet (UV) light, which can generate simultaneous autofluorescence and damage of biological systems besides to be opaque in living tissues [7, 12].

In order to overcome these drawbacks, ruthenium(II) polypyridyl complexes are versatile compounds typically used in several research fields due to their tunable photophysical and photochemical properties been attractive for applications in solar cells [13], biosensores [14], bioimaging [15], catalysis [16], PDT [17], among others. In addition, Ru(II) polypyridyl complexes are used as *d*-block chromophores to generate sensitized luminescence from Ln(III) ions with low energy *f f* excited states [12, 18 21]. The long-lived excited states known as triplet metal-to-ligand charge-transfer

(^{3}MLCT) possesses high absorption of visible light suitable to match the low energy *f f* excited states been efficient sensitizers for NIR-emitting Nd(III)/Yb(III) ions [22]. Several research groups have reported the synthesis of Ru Ln heterobinuclear complexes as strategy to overcome the limitation of UV excitation [12, 18 20, 22 25]. Although these complexes exhibit efficient sensitized NIR-emitting lanthanides by monitoring the excitation on ^{3}MLCT of Ru(II) moieties, the most of them show low solubility and transport in aqueous or biological media making it difficult to apply them as luminescent sensors and markers.

In this sense, mesoporous silica matrices appear as a good and fashionable alternative to explore luminescent properties of metal complexes in biological applications. Specifically, mesoporous silica nanoparticles (MSNs) exhibit low toxicity, good biodistribution, biodegradability and easy elimination make them suitable for *in vitro* and *in vivo* assays [26 28]. Beyond that, tunable physico-chemical properties as chemical stability, size, pores volume and
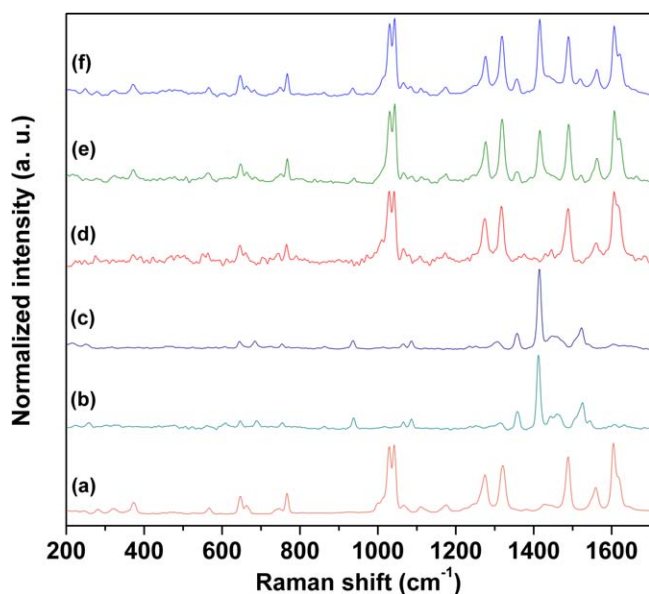
Figure 1. Raman scattering spectra of (a) RuL1, (b) YbL3, (c) NdL3, (d) SiO$_2$_Ru, (e) SiO$_2$_RuYb and (f) SiO$_2$_RuNd.

diameter, morphology, loading and release capacities, hydroxyl groups available and surface modification (inner and outer of pores) become them interesting nanoplatforms for cargo protection against premature leakage, deactivation processes and fast degradation [28_30]. Menu *et al* [31_36] have demonstrated the preparation of several luminescent silica-based nanohybrids and their successfully application as nanomarkers on *in vitro* assays [34, 36].

Herein, as a strategy to explore the potential of the Ru(II) and Nd/Yb(III) complexes and the advantages of the MSNs, we report the fabrication of three new luminescent silica-based nanohybrids: (i) **RuL1** grafting onto **MSNs** (labeled **SiO$_2$–Ru**) and (ii) simultaneous grafting of **RuL1** and **NdL3** or **YbL3** onto **MSNs** (labeled **SiO$_2$–RuNd** and **SiO$_2$_RuYb**, respectively). Structural characterization are successfully performed by using FT-RAMAM, SS-NMR and STEM techniques confirming the chemical integrity and the grafting of all complexes inside **MSNs** nanopores. Photophysical properties of **SiO$_2$–RuNd** and **SiO$_2$_RuYb** nanohybrids are studied and discussed in this work regarding to the efficiency of energy transfer processes from Ru(II) to NIR-emitting Nd/Yb(III) moieties when both *d* and *f* complexes are submitted to the silica nanopores. The **SiO$_2$–RuNd** and **SiO$_2$–RuYb** are exhibited as a promising dual (NIR_visible)-emitting nanotools for biomedical applications as nanosensors and nanomarkers.

2. Experimental

2.1. Materials

All reagents were purchased from Acros, Aldrich, SDS, New Biochem, Fluka, or Quimis and were used as received. The **RuL1** silylated complex were synthesized and successfully characterized as described in previous work [35, 36]. The

NdL3 and **YbL3** silylated complexes were synthesized similarly as previously described [33]. All silylated complexes are shown in scheme 1(a). Spherical mesoporous SiO$_2$ nanoparticles (labeled **MSNs**) was obtained as described by Nandiyanto *et al* [37]. MSNs with an average size of 47 $\pm$ 5 nm, a specific surface area value (S_{BET}) of 675 m^2 g^{-1} and average pore size of 9 nm were obtained. Dichloromethane and ethanol were purified by distillation in an inert atmosphere before use. The Schlenk system was used to prevent the hydrolysis reaction of the alkoxysilyl groups in the grafting reactions.

2.2. Characterization

Elemental analyses of C, H, N and S were performed on a Fisons EA1108 Instrument CHNS/O elemental analyzer. Nitrogen and Sulfur contents allow the determination of the grafting ratio, R, expressed in millimoles of complex per gram of silica. Nitrogen adsorption isotherms were measured on a Surface and Porosity Analyser Tristar 3020 Micromeritics apparatus, and the experiments were carried out on samples degassed at 90 °C under vacuum for 20 h. Surface areas were determined from the BET method. The presence of lanthanides and ruthenium on the mesoporous SiO$_2$ nanoparticles were evaluated by HR-TEM and STEM, using a JEOL JEM-ARM200F Cold FEG_EDS/EELS microscope. A drop of sol was diluted in ethanol. A carbon-coated grid was dipped in the solution and allowed to air-dry at room temperature. Raman spectra of the samples were collected on a RFS 100 Fourier transformed Raman Bruker spectrometer equipped with a Ge detector using liquid nitrogen as the coolant and a Nd:YAG laser emitting at 1064 nm. For each spectrum, an average of 1024 scans was performed at a resolution of 4 cm^{-1} over a range from 3500 to 50 cm^{-1}. The ^{29}Si{^{1}H}CP-MAS and ^{13}C{^{1}H}CP-MAS spectra were obtained on a Ascend III 400WB HD spectrometer, operating at 9.4 T, using a commercial 4 mm double resonance MAS-NMR probe. The frequencies of nuclei are 400.13, 79.49 and 100.6 MHz for ^{1}H, ^{29}Si and ^{13}C and spinning speeds of 15 and 10 kHz, respectively. ^{29}Si{^{1}H}CP-MAS spectra were measured with ^{1}H 90° pulse length of 2.9 μs, a contact time of 2.5 ms, and a relaxation delay of 5 s. ^{13}C{^{1}H}CP-MAS spectra were measured with ^{1}H 90° pulse length of 3.1 μs, a contact time of 3.5 ms, and a relaxation delay of 5 s. All spectra were acquired with TPPM proton decoupling during the data acquisition applying decoupling pulses of 5.8 μs length (π pulses). Chemical shifts are reported relative to TMS. Luminescence spectra were measured at room temperature using a Jobin-Yvon Model Fluorolog FL3-22 spectrometer equipped with a H10330-75 Hamamatsu detector, TE: cooled NIR-photomultiplier module and a 450 W Xe excitation lamp. Excitation and emission spectra were recorded under CW excitation and were corrected with respect to the Xe Lamp intensity and spectrometer response. Fluorescence intensity decays for the nanohybrids were obtained using the time-correlated single-photon counting technique. The excitation source was a mode-locked Ti:sapphire laser (Tsunami 3950 pumped by Millennia X Spectra
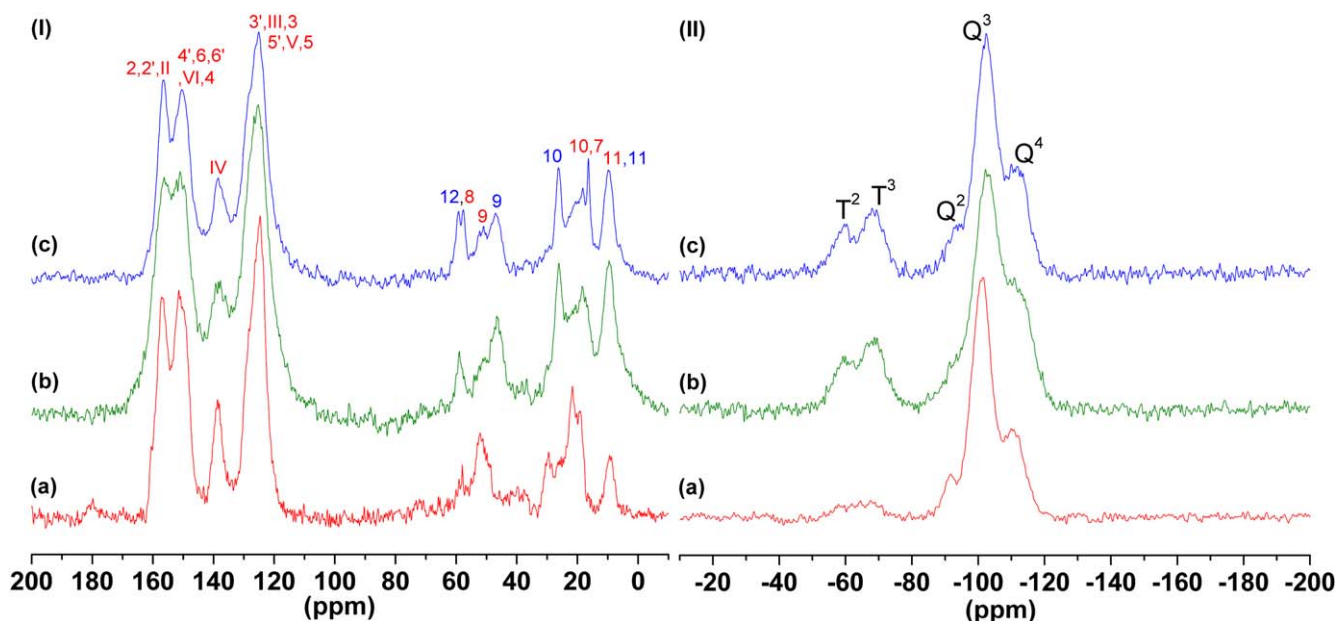
Figure 2. $^{13}C\{^1H\}$CP MAS NMR (I) and $^{29}Si\{^1H\}$CP MAS NMR spectra (II) of (a) SiO_2 Ru, (b) SiO_2 RuYb and (c) SiO_2 RuNd. 12: carbon atoms in methoxysilyl groups not grafted (Described the numbers in red and blue).
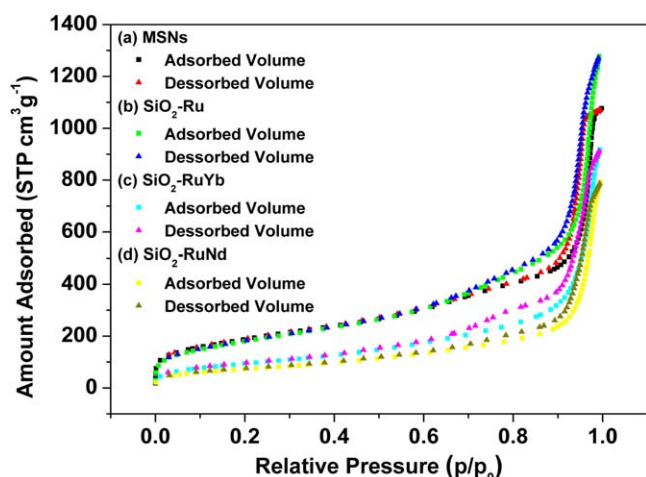

Figure 3. Nitrogen adsorption/desorption isotherms of (a) MSNs and (b) SiO_2 Ru, (c) SiO_2 RuYb and (d) SiO_2 RuNd nanohybrids.

Physics) producing 5 ps FWHM pulses ranging from 0.5 to 8.0 MHz repetition rate, regulated by the 3980 Spectra Physics pulse picker. The laser was tuned to give output at 892 nm and a second harmonic generator BBO crystal (GWN-23PL Spectra Physics) gave the 448 nm excitation pulses that were directed to an Edinburgh FL900 spectrometer adjusted in L-format configuration. The solid samples were placed in a holder perpendicular to the excitation source. The emission wavelength at 610 nm was selected by a monochromator and emitted photons were detected by a cooled Hamamatsu R3809U microchannel plate photomultiplier. The whole instrument response function was typically 100 ps. Energy transfer rate constant (k_{EnT}) and efficiency of energy transfer (η_{EnT}) were obtained using ruthenium ^{3}MLCT decay values from the **SiO₂–Ru** (used as a standard) and the **SiO₂–RuNd** and **SiO₂ RuYb** nanohybrids.

2.3. Synthesis

Two types of luminescent nanohybrids were obtained. First, by grafting of one complex (**RuL1**) onto MSNs (labeled **SiO₂–Ru**) and second, by simultaneously grafting of two complexes (**RuL1/NdL3** or **RuL1/YbL3**) onto MSNs (labeled **SiO₂–RuNd** and **SiO₂ RuYb**), schemes 1(b) and (c).

2.3.1. SiO₂–Ru nanohybrid.
0.32 mmol (285 mg) of **RuL1** complex was dissolved in ethanol (10 ml) and reacted with (285 mg) MSNs. The mixtures were stirred for 72 h at 295 K in N₂ atmosphere. The resulting suspensions were dialyzed for 72 h, and the solids were isolated by centrifugation at 15 000 rpm for 15 min The SiO₂ Ru obtained was washed with water, ethanol and diethyl ether. All solids obtained were dried under vacuum for 4 h. **SiO₂ Ru:** Elemental analysis %, found (calcd): $R = 0.18$ mmol g ^{1}: C, 10.51 (8.98); H, 1.29 (0.90); N, 1.05 (1.05).

2.3.2. SiO₂–RuNd and SiO₂–RuYb nanohybrids.
0.20 mmol (178 mg) of **RuL1** complex, 0.20 mmol (260 mg) of **NdL3** complex and 0.20 mmol (289 mg) of **YbL3** complex were dissolved in ethanol (20 ml) and reacted with (450 mg) MSNs. The mixtures were stirred for 72 h at 295 K in an N₂ atmosphere. The resulting suspensions were dialyzed for 72 h, and the solids were isolated by centrifugation at 15 000 rpm for 15 min The obtained solids were washed with water, ethanol, dichloromethane, and diethyl ether and then dried under vacuum for 4 h. **SiO₂ RuNd:** Elemental analysis %, found (calcd): $R_{Ru} = 0.14$ mmol g ^{1} and $R_{Nd} = 0.16$ mmol g ^{1}: C, 15.34 (14.65); H, 1.74 (1.54); N, 1.32 (1.32); S, 1.53 (1.53). **SiO₂ RuYb:** Elemental analysis %, found (calcd): $R_{Ru} = 0.11$ mmol g ^{1} and

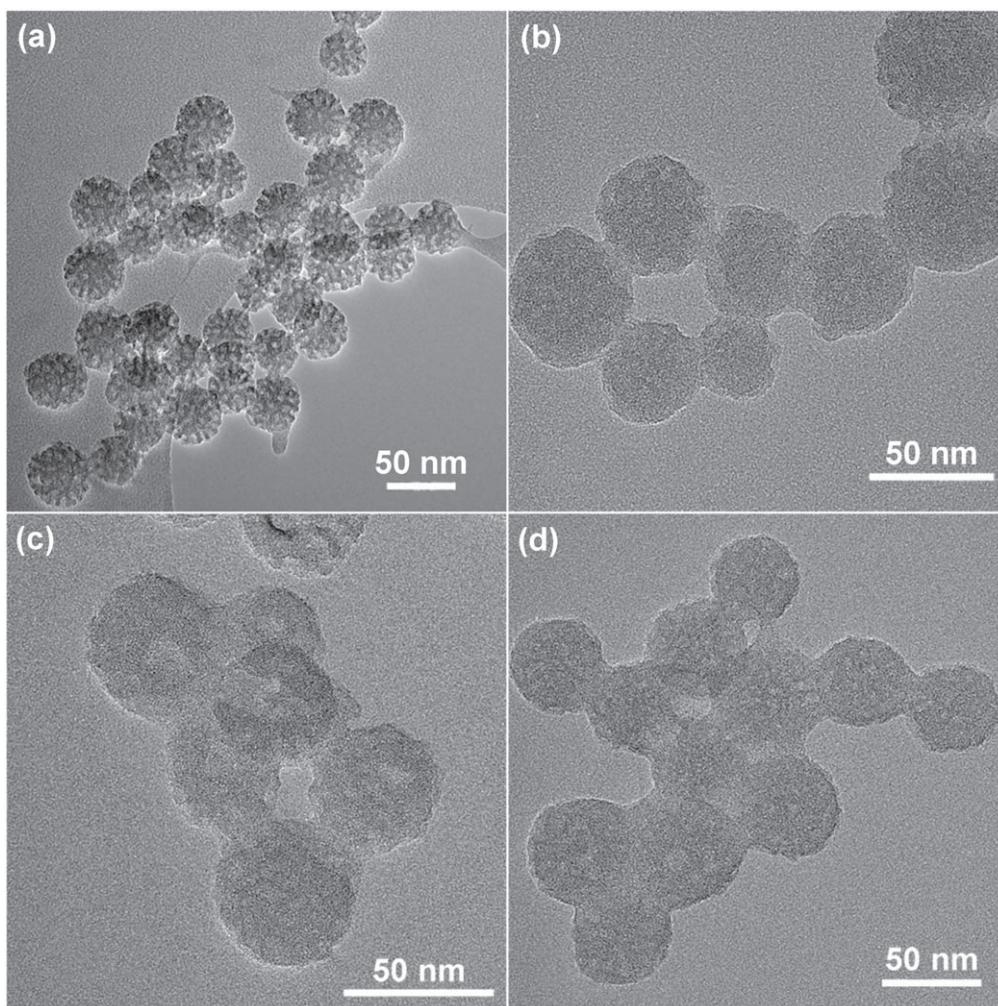**Figure 4.** HR TEM images of (a) MSNs and different nanohybrids: (b) SiO_2 Ru, (c) SiO_2 RuYb and (d) SiO_2 RuNd.

R_{Yb} = 0.15 mmol g^{-1}: C, 15.52 (12.67); H, 1.74 (1.34); N, 1.05 (1.05); S, 1.41 (1.41).

3. Results and discussion

3.1. Characterization of the silica-based nanohybrids

RuL1 complex (scheme 1(a, i)) and **LnL3** (Ln = Nd(III), Yb(III)) complexes are displayed in schemes 1(a, i) and (a, ii), respectively. The silica-based nanohybrids labeled **SiO$_2$–Ru** and **SiO$_2$–RuLn** were successfully prepared as shown in schemes 1(b) and (c), respectively.

FT-RAMAN measurements show characteristic bands ascribed to the complexes and bands relating to Ln O and Ru N bonds. Figure 1 displays Raman scattering similar spectra obtained for **SiO$_2$-Ru** (figure 1(a)), **SiO$_2$–RuYb** (figure 1(b)) and **SiO$_2$–RuNd** (figure 1(c)) nanohybrids

The characteristic bands of the **RuL1** and **LnL3** complexes were detected also in the nanohybrids as displayed in figure 1. Bands in the 640 685 cm^{-1} region were assigned to ν(Ln O) and ν(Ru N) from **LnL3** and **RuL1** complexes, respectively [38 41]. Additionally, at 372 and 1030 1045

cm^{-1} bands attributed to ν(Ru N) were detected [40, 41]. Bands observed at 1605 1629 cm^{-1} were ascribed to ν(C=N) and at 1490 and 1560 cm^{-1} assigned to ν(C=C) present in the **RuL1** complex. Bands relating to **LnL3** complexes were found at 1357 and 1415 cm^{-1} corresponding to ν(C=O and C=C) [38, 39]. These results corroborate DRIFT analysis (not show) confirming **RuL1** and **LnL3** complexes grafted onto MSNs.

The chemical integrity of the complexes grafted onto MSNs was verified by ^{13}C{^{1}H}CP-MAS NMR spectroscopy. Figure 2(I) shows ^{13}C{^{1}H}CP-MAS spectra for the nanohybrids obtained by grafting of **RuL1** and **LnL3** complexes. The spectrum ascribed to the **SiO$_2$ Ru** nanohybrid (figure 2(I, a)) shows signals of carbon atoms of the **RuL1** complexes grafted in the silica matrix. Signals at 125, 139, 151 and 157 ppm were attributed to the carbon atoms of the bpy ligands, CIII-CV, CIV, CVI and CII, respectively [36]. The signals ascribed to the carbon atoms of the propyl chain were observed with low intensity at 10 (C11), 22 (C10 and C7), 55 (C9) and 58 (C8) ppm [36]. It is worth noting that the characteristic signals expected from TTA ligands were not observed in the figures 2(I, b and c). The low sensibility in both spectra (figures 2(I, b and c)) can be ascribed to the
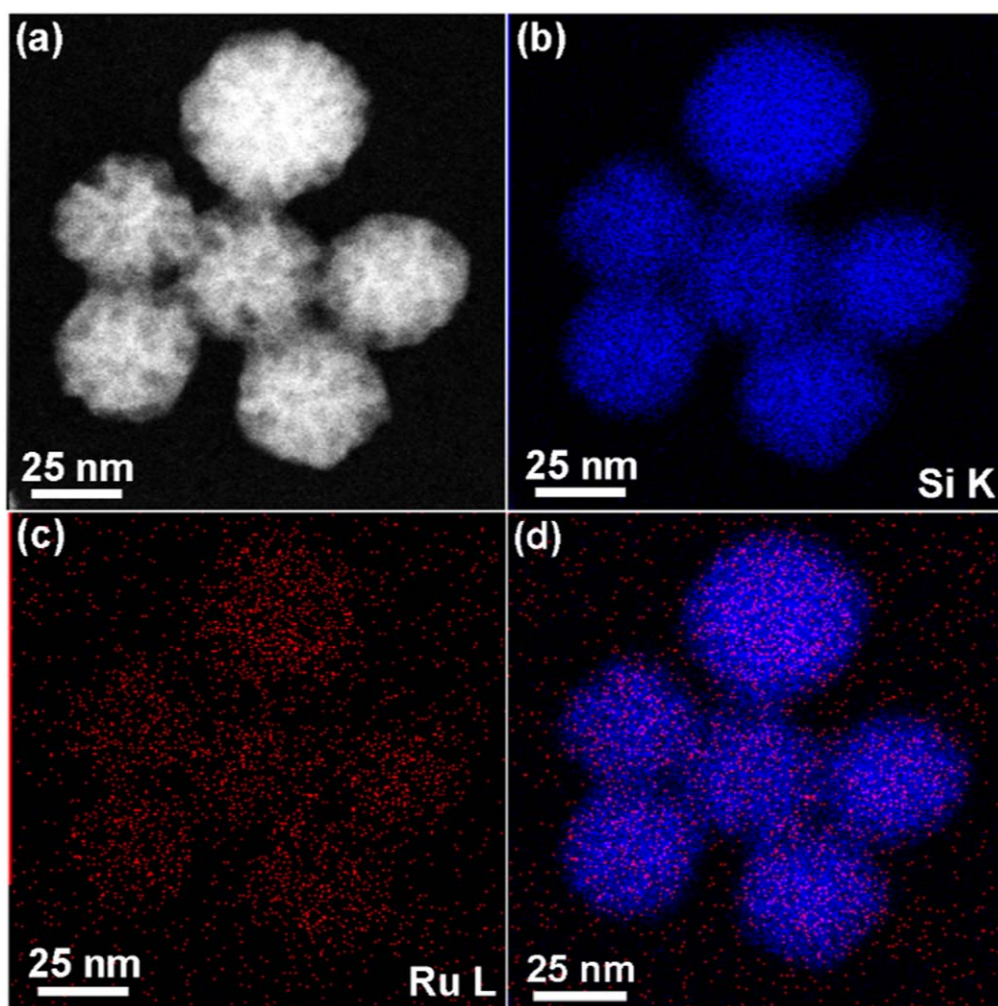
Figure 5. Electron microscope images and elemental mapping of the SiO$_2$ Ru: (a) STEM image, (b) Si mapping, (c) Ru mapping and (d) Si (blue color) and Ru (red color) mapping.

paramagnetic interactions, compromising the efficiency of the cross-polarization process owing to very short ^{1}H spin-lattice relaxation times in the rotating frame [42]. For the **SiO$_2$ RuNd** and **SiO$_2$–RuYb** nanohybrids (figures 2(I, b and c)), only signals ascribed to the bpy ligands, ethoxysilyl and methoxysilyl groups, present in the ruthenium and lanthanide complexes could be observed. The spectra were similar for both nanohybrids with signals at 125, 139, 151 and 157 ppm assigned to the carbon atoms of the bpy ligands, CIII-CV, CIV, CVI and CII, respectively, for the ruthenium complexes. Signals at 10, 22, 55 and 58 ppm, C11, C10-C7, C9 and C8, respectively, were attributed to the ethoxysilyl groups present in the **RuL1** complexes. The signals at 47, 26 and 10 ppm were ascribed to the carbon atoms of the methoxysilyl groups, C9, C10 and C11, respectively, present in the **LnL3** complexes. Methoxysilyl groups not grafted were detected in figures 2 (I, c) and assigned to C12.

Figure 3 shows nitrogen adsorption/desorption isotherms from **MSNs**, **SiO$_2$ Ru**, **SiO$_2$–RuYb** and **SiO$_2$ RuNd** samples that exhibits a type IV shape, which is characteristic of mesoporous materials [35]. Values of specific surface area (S_{BET}) of the **SiO$_2$–Ru** nanohybrids ($S_{BET} = 654$ m^2 g^{-1})

decreased relating to the **MSNs** ($S_{BET} = 675$ m^2 g^{-1}). For the **SiO$_2$–RuYb** and **SiO$_2$–RuNd**, these values of S_{BET} decreased significantly with 348 and 268 m^2 g^{-1}, respectively, confirming that the nanopores are filled up with complexes.

HR-TEM measurements were carried out to evaluate the morphology and nanopores structure after grafting of the silylated complexes. Figure 4 shows HR-TEM images of the **MSNs** (a) and **SiO$_2$–Ru** (b), **SiO$_2$–RuYb** (c) and **SiO$_2$–RuNd** (d) nanohybrids. The MSNs (figure 4(a)) displays a random distribution of the nanopores clearly observed as previously described [37]. However, according to the HR-TEM images, all nanohybrids present spherical morphology without changing of the structure besides show the nanopores filled up, confirming the most of complexes are grafting inside de nanopores. These results corroborate DRIFT, FT-RAMAN, N$_2$ adsorption/desorption and solid-state NMR analysis exhibiting the presence of the complexes inside de nanopores of the matrices.

In STEM measurements, atoms with high electron density as ruthenium, neodymium and ytterbium can be easily distinguished from Si atoms. The elemental mapping were obtained by EDX spectroscopy on STEM microscopy, and
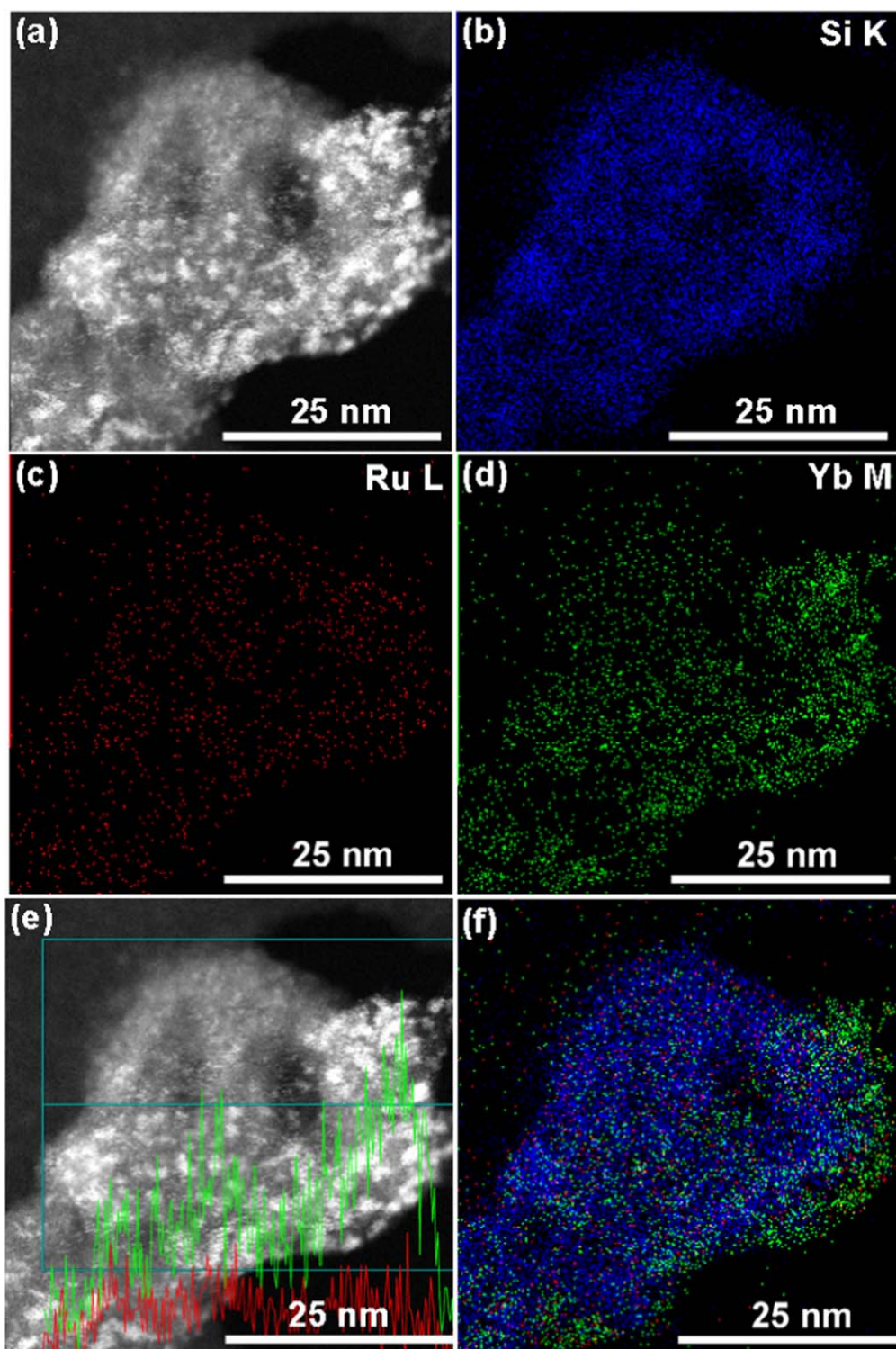
Figure 6. Electron microscope images and elemental mapping of the SiO_2 RuYb: (a) STEM image, (b) Si mapping, (c) Ru mapping, (d) Yb mapping, (e) Si (blue color), Ru (red color) and Yb (green color) mapping. (f) STEM image with a line profile of Ru (red line) and Yb (green line) atoms in the selected area (blue line).

the obtained results for **SiO_2 Ru**, **SiO_2–RuYb** and **SiO_2 RuNd** are shown in figures 5 7

  SiO_2–Ru nanohybrid kept the spherical shape. Elemental mapping of Si atoms confirm that these elements are homogenously dispersed to form the **MSNs**. Ru atoms are also detected and its appear homogenously well dispersed inside the nanopores. Grafting efficiency observed by STEM are in agreement with the EA data (**SiO_2–Ru:** 0.18 mmol g ^{1} of silica).

  SiO_2–RuYb and **SiO_2–RuNd** nanohybrids displayed grafting efficiencies higher than **SiO_2–Ru** nanohybrid discussed above due to the grafting of two types of complexes onto **MSNs**. Concerning **SiO_2 RuYb** and **SiO_2 RuNd**
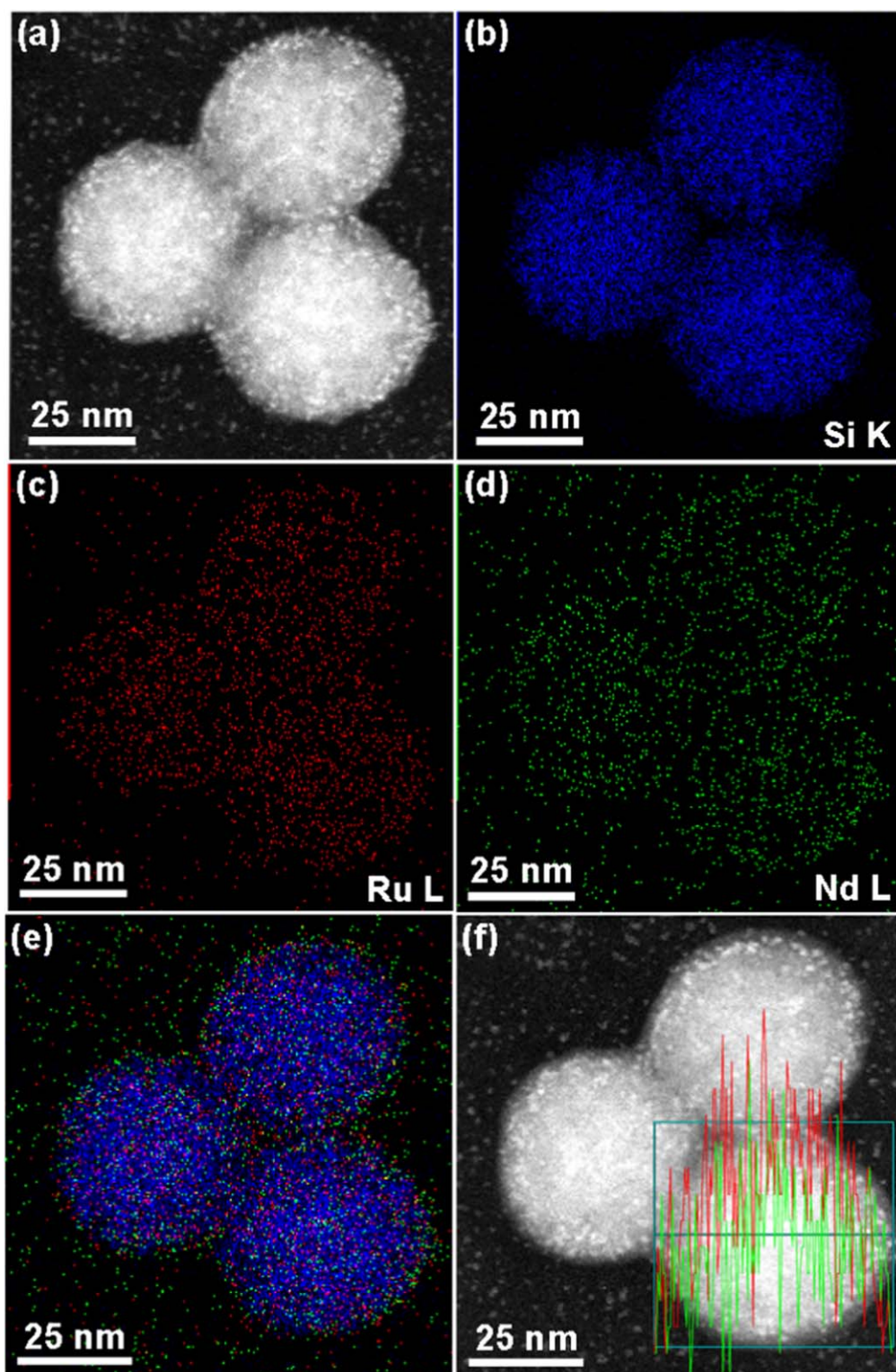
Figure 7. Electron microscope images and elemental mapping of the SiO$_2$ RuNd: (a) STEM image, (b) Si mapping, (c) Ru mapping, (d) Nd mapping and (e) Si (blue color), Ru (red color) and Nd (green color) mapping. (f) STEM image with a line profile of Ru (red line) and Nd (green line) atoms in the selected area (blue line).

nanohybrids, elemental mapping of Si atoms confirms that these elements are homogenously dispersed to form the **MSNs**.

Figure 6 exhibits Ru and Yb atoms appear heterogeneously distributed inside and at the surface of the MSNs nanopores. The higher Yb concentration compared with Ru

atoms at the nanoparticles surface is in agreement with the EA data (SiO$_2$ RuYb: 0.11 and 0.15 mmol g^{-1} of silica using N and S contents for the calculation, respectively).

On the other hand, concerning **SiO$_2$–RuNd**, Ru and Nd atoms are homogenously dispersed inside the nanopores
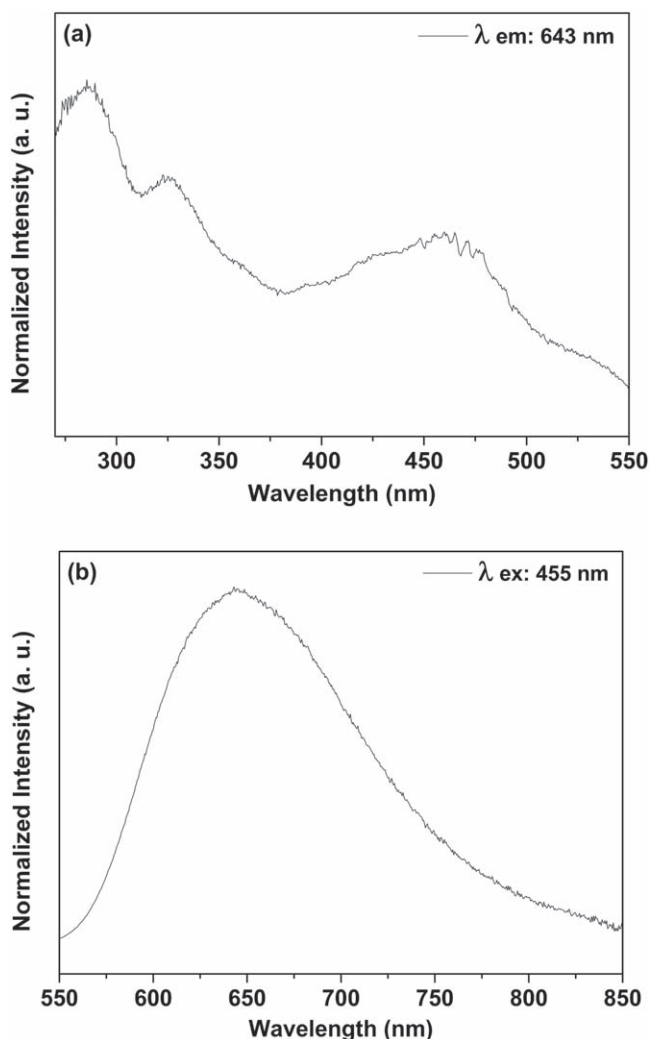
Figure 8. Room temperature excitation ((a), $\lambda_{emission} = 643$ nm) and emission ((b), $\lambda_{excitation} = 455$ nm) spectra of the SiO_2 Ru nanohybrid in solid state.

Table 1. Grafting efficiencies, in mmol of Ru(II) and Ln(III) complexes g^{-1} of silica, and amount of Ru(II) and Ln(III) complexes nm^{-2} of silica for the nanohybrids.

Samples	R (mmol g^{-1} of SiO_2)		Number of complex per nm^2	
	R_{Ru}	R_{Ln}	Ru	Ln
SiO_2 Ru	0.18		0.16	
SiO_2 RuYb	0.11	0.15	0.09	0.13
SiO_2 RuNd	0.14	0.16	0.12	0.14

(figure 7). STEM data confirm grafting efficiencies as obtained by EA (**SiO₂–RuNd**: 0.14 and 0.16 mmol g ^{1} of silica, calculated from Ru(II) and Nd(III) moieties, respectively).

The grafting of Ru(II) and Ln(III) complexes (in mmol of complex g ^{1} of silica) was calculated according to the N and S contents, respectively, as described by Menu *et al* [32, 33, 36]. The number of complexes nm^{2} of silica were calculated using grafting efficiency, Avogadro number and

specific surface area values of the matrix before grafting of the complexes as exhibited in table 1.

The grafting efficiencies using MSNs with 765 m^2 g ^{1} of silica were higher for **SiO₂ RuYb** and **SiO₂–RuNd** than for **SiO₂ Ru** nanohybrid. Additionally, 0.09 0.16 complexes per nm^2 were grafted onto **MSNs**. Despite similar concentration of **RuL1** and **LnL3** complexes added for grafting reactions, EA results display more grafted **LnL3** than **RuL1**, for both **SiO₂–RuYb** and **SiO₂–RuNd** nanohybrids.

3.2. Photophysical properties of the silica-based nanohybrids

Figure 8 shows the excitation (a) and emission (b) spectra from **SiO₂–Ru** nanohybrid. Bands at 285, 325 and 455 nm are observed in the excitation spectrum related to transitions centered on the ligand ($\pi \rightarrow \pi^*$ transitions) on the metal ($\pi_M \rightarrow \sigma^*_M$ transitions) and ^{1}MLCT ($d \rightarrow \pi^*$ transitions), respectively [35]. The characteristic emission band of **SiO₂ Ru** nanohybrid centered at 643 nm was ascribed to the transition from the ^{3}MLCT excited state to the ground state [35]. The blue shift compared to the free **RuL1** complex is related to the rigido-chromism phenomenon [43, 44] due the interaction between the complexes and the silanol groups of the rigid network avoid the spatial reorientation of complex. When **RuL1** complex was grafted onto mesoporous surface, the solvent present into the pores was unable to reorient around the excited complex. As a consequence, the Franck Condon excited state was not completely stabilized, and emission occurred from a higher energy level than free complex [35]. Luminescence spectra from **RuL1** (figure S1), **YbL3** (figure S2) and **NdL3** (figure S3) complexes are exhibited in the supplementary material.

Figure 9 shows excitation and emission spectra obtained from **SiO₂ RuYb** nanohybrid. A broad emission band was observed at 610 nm and assigned to the Ru(II) ^{3}MLCT emission [35] in a similar way observed for **SiO₂–Ru** (figure 8). Comparing with free **RuL1** complex, the ^{3}MLCT energy was blue shifted as previously described (**SiO₂–Ru** in the figure 8). The excitation spectra obtained by monitoring the Ru(II) ^{3}MLCT emission shows bands ascribed to the $d \rightarrow \pi^*$ ^{1}MLCT transitions, transitions centered on ligands ($\pi \rightarrow \pi^*$ transitions) and transitions centered on the metal ($\pi_M \rightarrow \sigma^*_M$ transitions), [35] in agreement with the free **RuL1** complex.

The IR emission band peaking at 980 nm with broader components at 1010 and 1030 nm (figure 9(d)) could be ascribed to the Yb(III) $^2F_{5/2} \rightarrow ^2F_{7/2}$ transition [45 47]. The excitation spectrum (figure 9(c)) shows the broad ligand centered band below 400 nm and the Ru(II) related band from 400 to 700 nm. Considering the excitation spectrum obtained by monitoring the Ru related visible emission, the sensitization of the Yb(III) IR emission is clearly shown here.

Figure 10 depicts results detected from **SiO₂–RuNd** nanohybrid. The Ru(II) related broad emission band is observed peaking at 610 nm (figure 10(b)). Excitation spectrum obtained by monitoring the broad emission bands shows the broad bands assigned to the ligands and Ru(II) in similar way obtained for the **SiO₂ RuYb**.
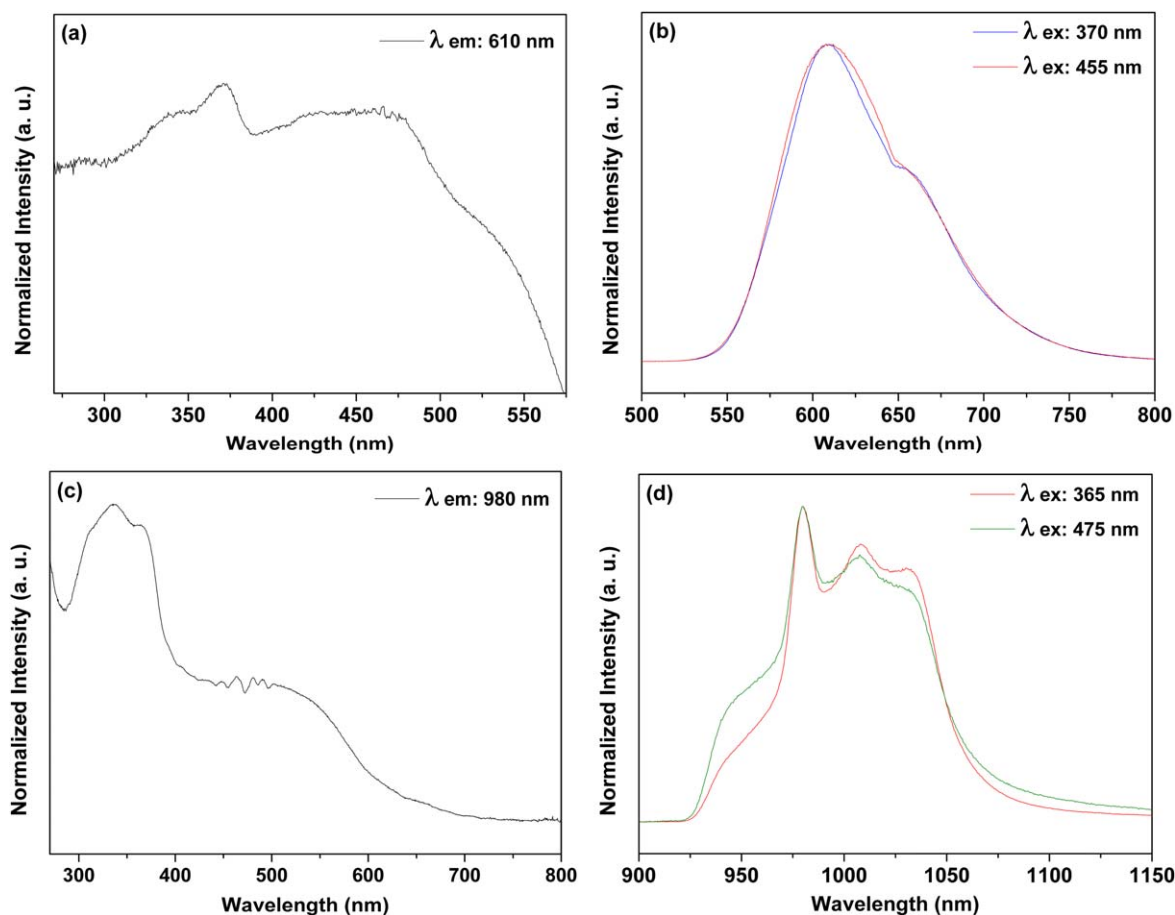
Figure 9. Room temperature excitation ((a), $\lambda_{\text{emission}}$: 610 nm and (c), $\lambda_{\text{emission}}$: 980 nm) and emission ((b), $\lambda_{\text{excitation}}$: 370 and 455; and (d), $\lambda_{\text{excitation}}$: 365 and 475 nm) spectra of the SiO_2 RuYb nanohybrid in solid state.

Two emission bands were detected in the infrared region at 1061.5 nm (attributed to Nd(III) $^4F_{3/2} \rightarrow {}^4I_{11/2}$ transition) and at 1333 nm (Nd(III) $^4F_{3/2} \rightarrow {}^4I_{13/2}$ transition) [45 47]. The excitation spectrum obtained when monitoring emission at 1061.5 shows Nd(III) above 700 nm. Two broad bands are observed below 600 nm. In the same way observed for the **SiO₂–RuYb** nanohybrid, here the Ru(II) to Nd(III) energy transfer is evidenced. The energy levels diagram presented in scheme 2 illustrates the observed energy transfer processes.

Decay time results observed for the Ru(II) MLCT level are presented in table 2. Decreasing decay times in the presence of lanthanide ions put in evidence Ru Ln energy transfer (EnT) processes.

Energy transfer rate of 0.11×10^7 s ^{1} and efficiency of energy transfer of 27.5% were obtained for **SiO₂–RuYb**. EnT rate of 0.20×10^7 s ^{1} and efficiency of energy transfer of 40% could be evaluated for **SiO₂–RuNd**. The higher values observed for the Nd(III) hybrid is well explained by the matching of donor and acceptor energy levels as shown in scheme 2.

Therefore, three new luminescent nanohybrids were prepared. The photophysical properties of **SiO₂ RuNd** and **SiO₂–RuYb** nanohybrids were evaluated and energy transfer processes were confirmed for lifetimes data obtained from Ru(II) emission decay and emission/excitation spectra.

4. Conclusion

We have fabricated three new luminescent silica-based nanohybrids by grafting of silylated Ru(II) and Nd/Yb(III) complexes onto MSNs. The silica matrix prepared by microemulsion method displayed interesting features for post modification such as high surface area with high porosity and silanol groups available, detected by HR-TEM, DRIFT, N_2 adsorption/desorption analysis. Structural characterization of all nanohybrids were successfully achieved by using DRIFT, FT-RAMAN, SS-NMR, HR-TEM and STEM techniques, confirming the presence of the Ru(II) and Nd/Yb(III) inside the SiO_2 nanopores. Luminescent properties were evaluated by monitoring the excitation on MLTC states from Ru(II) moieties. SiO_2 Ru nanohybrid displays the characteristic emission band at 643 nm. For SiO_2 RuNd and SiO_2 RuYb nanohybrids, emissions in the visible correspond to the Ru(II) complexes (from the ^{3}MLCT excited state) while the NIR emissions were assigned to the Nd(III) ($^4F_{3/2} \rightarrow {}^4I_{11/2}$ and $^4F_{3/2} \rightarrow {}^4I_{11/2}$ transitions) and Yb(III) ($^2F_{5/2} \rightarrow {}^2F_{7/2}$ transition) ions. From Decay times of the Ru(II) moieties in the SiO_2 RuNd and SiO_2 RuYb nanohybrids, energy transfer processes were revealed with k_{EnT} values of 0.20×10^7 and 0.11×10^7 s ^{1} and η_{EnT} of 40% and 27.5%, respectively. These results confirm Nd(III) levels more suitable for energy
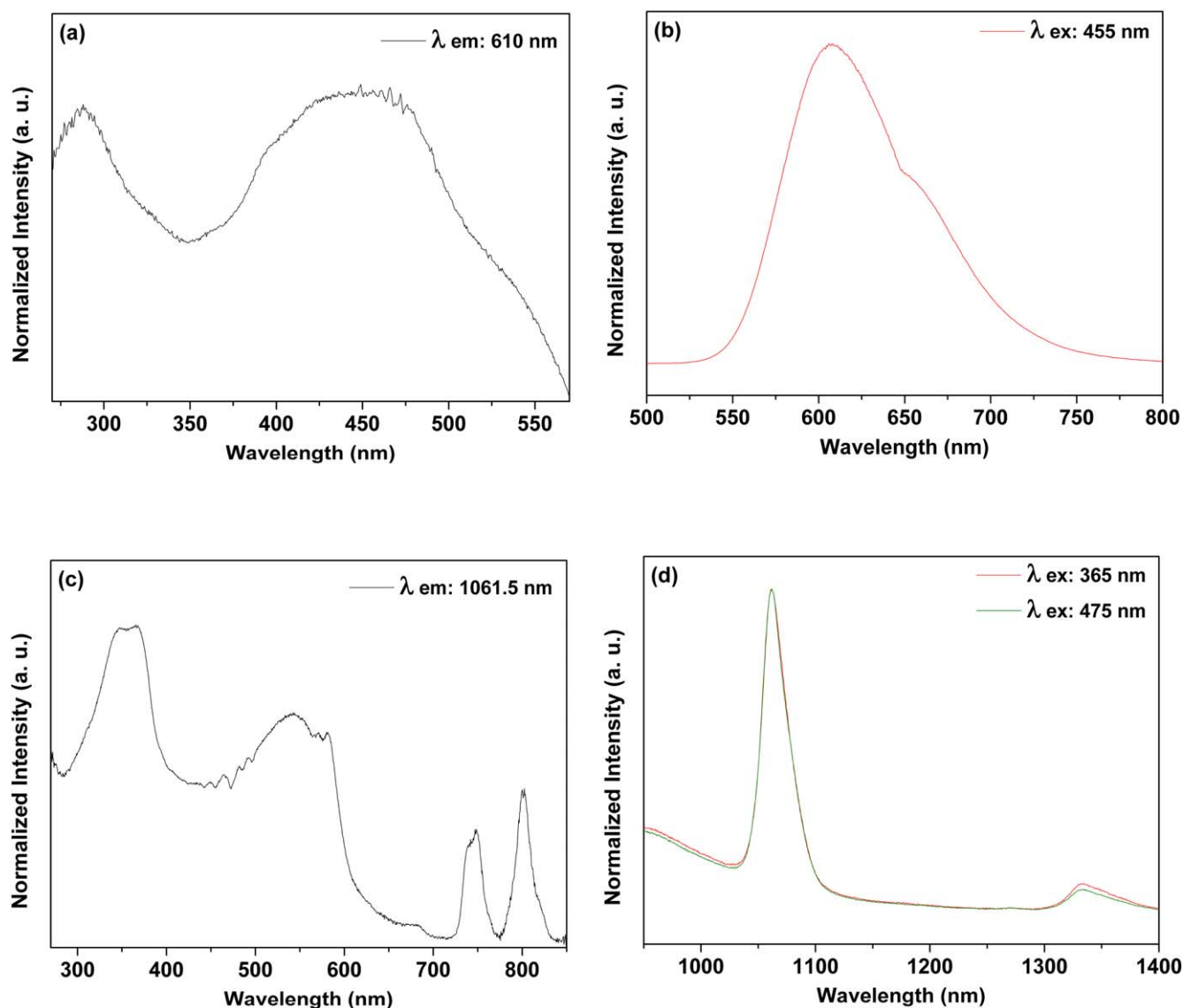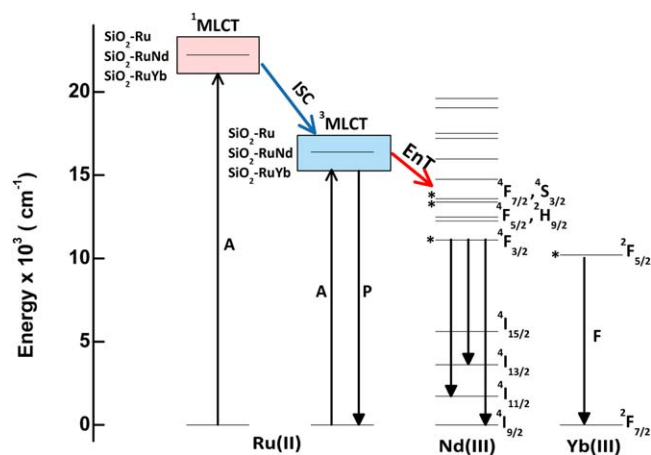
Figure 10. Room temperature excitation ((a), $\lambda_{\text{emission}}$: 610 nm and (c), $\lambda_{\text{emission}}$: 1061.5 nm) and emission ((b), $\lambda_{\text{excitation}}$: 390 and 455 nm; and (d), $\lambda_{\text{excitation}}$: 365 and 455 nm) spectra of the SiO_2 RuNd nanohybrid in solid state.

Scheme 2. Schematic energy transfer processes (Ru(II)) to Nd(III) and Yb(III) (A = Absorption; ISC = Inter System Cross; P = phosphorescence; EnT = energy transfer; F = Fluorescence) in the SiO_2 Ru, SiO_2 RuNd and SiO_2 RuYb nanohybrids.

Table 2. Photophysical properties for MLCT based visible emission and Ln(III) based NIR.

| | MLCT based emission (Ex: 448 nm) | | | |
	λ/nm	τ/ns	[a]$k_{\text{EnT}}/10^7$ s^{-1}	[b]$\eta_{\text{EnT}}/\%$
SiO_2 Ru	610	344.7		
SiO_2 RuNd	610	206.2	0.20	40.2
SiO_2 RuYb	610	249.8	0.11	27.5

[a] k_{EnT} (energy transfer rate constant) $1/\tau_q$ $1/\tau_u$ (τ_q and τ_u refer to the 'quenched' and 'unquenched' lifetime of Ru(II) complexes before and after coordination with Ln(III)).
[b] η_{EnT} (efficiency of energy transfer) 1 (τ_q/τ_u).

transfer than Yb(III) from Ru(II) ^{3}MLTC excited states. Finally, the photophysical investigation suggests the dual (NIR/visible)-emitting SiO_2 RuNd and SiO_2 RuYb nanohybrids as potential nanolabels for biological assays.

ORCID iDs

Rafael Miguel Sábio ⬤ https://orcid.org/0000-0002-3852-2184

References

[1] Bunzli J C G and Piguet C 2005 Taking advantage of luminescent lanthanide ions *Chem. Soc. Rev.* **34** 1048 77

[2] Carlos L D, Ferreira R A S, Bermudez V, de Z and Ribeiro S J L 2009 Lanthanide containing light emitting organic inorganic hybrids: a bet on the future *Adv. Mater.* **21** 509 34

[3] Bünzli J C G 2015 On the design of highly luminescent lanthanide complexes *Coord· Chem. Rev.* **293 294** 19 47

[4] Bünzli J C G and Eliseeva S V 2010 Lanthanide NIR luminescence for telecommunications, bioanalyses and solar energy conversion *J. Rare Earths* **28** 824 42

[5] Huang P, Zheng W, Zhou S, Tu D, Chen Z, Zhu H, Li R, Ma E, Huang M and Chen X 2014 Lanthanide doped LiLuF$_4$ upconversion nanoprobes for the detection of disease biomarkers *Angew. Chem., Int. Ed.* **53** 1252 7

[6] Ma Q, Wang J, Li Z, Lv X, Liang L and Yuan Q 2019 Recent progress in time resolved biosensing and bioimaging based on lanthanide doped nanoparticles *Small* 1804969

[7] Bünzli J C G 2016 Lanthanide light for biology and medical diagnosis *J. Lumin.* **170** 866 78

[8] Clough T J, Jiang L, Wong K L and Long N J 2019 Ligand design strategies to increase stability of gadolinium based magnetic resonance imaging contrast agents *Nat. Commun.* **10** 1420

[9] Sun X *et al* 2019 Noninvasive temperature monitoring for dual modal tumor therapy based on lanthanide doped up conversion nanocomposites *Biomaterials* **201** 42 52

[10] Feng Y, Wu Y, Zuo J, Tu L, Que I, Chang Y, Cruz L J, Chan A and Zhang H 2019 Assembly of upconversion nanophotosensitizer *in vivo* to achieve scatheless real time imaging and selective photodynamic therapy *Biomaterials* **201** 33 41

[11] Hamblin M R and Demidova T N 2006 Mechanisms of low level light *Proc. SPIE* **6140** 614001

[12] Chen F F, Chen Z Q, Bian Z Q and Huang C H 2010 Sensitized luminescence from lanthanides in d f bimetallic complexes *Coord· Chem. Rev.* **254** 991 1010

[13] Wang P, Zakeeruddin S M, Moser J E, Nazeeruddin M K, Sekiguchi T and Grätzel M 2003 A stable quasi solid state dye sensitized solar cell with an amphiphilic ruthenium sensitizer and polymer gel electrolyte *Nat. Mater.* **2** 402 7

[14] Gill M R and Thomas J A 2012 Ruthenium(ii) polypyridyl complexes and DNA from structural probes to cellular imaging and therapeutics *Chem. Soc. Rev.* **41** 3179

[15] Gill M R, Garcia Lara J, Foster S J, Smythe C, Battaglia G and Thomas J A 2009 A ruthenium(II) polypyridyl complex for direct imaging of DNA structure in living cells *Nat. Chem.* **1** 662 7

[16] Farney E P, Chapman S J, Swords W B, Torelli M D, Hamers R J and Yoon T P 2019 Discovery and elucidation of counteranion dependence in photoredox catalysis *J. Am. Chem. Soc.* **141** 6385 91

[17] Albani B A, Peña B, Leed N A, de Paula N A B G, Pavani C, Baptista M S, Dunbar K R and Turro C 2014 Marked improvement in photoinduced cell death by a new tris heteroleptic complex with dual action: singlet oxygen sensitization and ligand dissociation *J. Am. Chem. Soc.* **136** 17095 101

[18] Lazarides T, Adams H, Sykes D, Faulkner S, Calogero G and Ward M D 2008 Heteronuclear bipyrimidine bridged Ru Ln and Os Ln dyads: low energy ^{3} MLCT states as energy donors to Yb(iii) and Nd(iii) *Dalton Trans.* **0** 691 8

[19] Lazarides T, Sykes D, Faulkner S, Barbieri A and Ward M D 2008 On the mechanism of d f energy transfer in RuII/LnIII and OsII/LnIII dyads: dexter type energy transfer over a distance of 20 Å *Chemistry Eur. J.* **14** 9389 99

[20] Lazarides T, Tart N M, Sykes D, Faulkner S, Barbieri A and Ward M D 2009 [Ru(bipy)$_3$]$_{2+}$ and [Os(bipy)$_3$]$_{2+}$ chromophores as sensitisers for near infrared luminescence from Yb(iii) and Nd(iii) in d/f dyads: contributions from Förster dexter, and redox based energy transfer mechanisms *Dalton Trans.* 3971 9

[21] Ward M D 2007 Transition metal sensitised near infrared luminescence from lanthanides in d f heteronuclear arrays *Coord· Chem. Rev.* **251** 1663 77

[22] Ward M D 2010 Mechanisms of sensitization of lanthanide (III) based luminescence in transition metal/lanthanide and anthracene/lanthanide dyads *Coord· Chem. Rev.* **254** 2634 42

[23] Zhang L Y, Hou Y J, Pan M, Chen L, Zhu Y X, Yin S Y, Shao G and Su C Y 2015 Near infrared (NIR) emitting Nd/Yb(III) complexes sensitized by MLCT states of Ru(II)/Ir (III) metalloligands in the visible light region *Dalton Trans.* **44** 15212 9

[24] Wei Q H, Lei Y F, Xu W R, Xie J M and Chen G N 2012 Ru (ii) sensitized lanthanide luminescence: synthesis, photophysical properties, and near infrared luminescent determination of alpha fetal protein (AFP) *Dalton Trans.* **41** 11219

[25] Singaravadivel S, Babu E, Velayudham M, Lu K L and Rajagopal S 2013 Sensitized near infrared luminescence of NdIII, YbIII and ErIII complexes by energy transfer from a ruthenium antenna *J. Organomet. Chem.* **738** 49 54

[26] Maturi F *et al* 2019 Luminescent mesoporous silica nanohybrid based on drug derivative terbium complex *Materials* **12** 933

[27] Lu J, Liong M, Li Z, Zink J I and Tamanoi F 2010 Biocompatibility, biodistribution, and drug delivery efficiency of mesoporous silica nanoparticles for cancer therapy in animals *Small* **6** 1794 805

[28] Sábio R M, Meneguin A B, Ribeiro T C, Silva R R and Chorilli M 2019 New insights towards mesoporous silica nanoparticles as a technological platform for chemotherapeutic drugs delivery *Int. J. Pharm.* **564** 379 409

[29] Rocha L A, Do J, Freiria C, Maurício J, Caiut A, Ribeiro S J L, Messaddeq Y, Verelst M and Dexpert Ghys J 2015 Luminescence properties of Eu complex formations into ordered mesoporous silica particles obtained by the spray pyrolysis process *Nanotechnology* **26** 335604

[30] Rocha L A, Caiut J M A, Messaddeq Y, Ribeiro S J L, Martines M A U, Freiria J, do C, Dexpert Ghys J and Verelst M 2010 Non leachable highly luminescent ordered mesoporous SiO$_2$ spherical particles *Nanotechnology* **21** 155603

[31] Cousinié S, Gressier M, Reber C, Dexpert Ghys J and Menu M J 2008 Europium(III) complexes containing organosilyldipyridine ligands grafted on silica nanoparticles *Langmuir* **24** 6208 14

[32] Cousinié S, Mauline L, Gressier M, Kandibanda S R, Datas L, Reber C and Menu M J 2012 Bulk or surface grafted silylated Ru(ii) complexes on silica as luminescent nanomaterials *New J. Chem.* **36** 1355

[33] Duarte A P, Gressier M, Menu M J, Dexpert Ghys J, Caiut J M A and Ribeiro S J L 2012 Structural and luminescence properties of silica based hybrids containing new silylated diketonato Europium(III) complex *J. Phys. Chem.* C **116** 505 15

[34] Duarte A P *et al* 2013 Organosilylated complex [Eu(TTA)3 (Bpy Si)]: a bifunctional moiety for the engeneering of luminescent silica based nanoparticles for bioimaging *Langmuir* **29** 5878 88

[35] Sábio R M, Gressier M, Caiut J M A, Menu M J and Ribeiro S J L 2016 Luminescent multifunctional hybrids obtained by grafting of ruthenium complexes on mesoporous silica *Mater. Lett.* **174** 1 5

[36] Mauline L, Gressier M, Roques C, Hammer P, Ribeiro S J L, Caiut J M A and Menu M J 2013 Bifunctional silica nanoparticles for the exploration of biofilms of *Pseudomonas aeruginosa Biofouling* **29** 775 88

[37] Nandiyanto A B D, Kim S G, Iskandar F and Okuyama K 2009 Synthesis of spherical mesoporous silica nanoparticles with nanometer size controllable pores and outer diameters *Microporous Mesoporous Mater.* **120** 447 53

[38] Malta O L, Brito H F, Menezes J F S, Silva F R G E, Alves S, Farias F S and de Andrade A V M 1997 Spectroscopic properties of a new light converting device Eu(thenoyltrifluoroacetonate)3 2(dibenzyl sulfoxide). A theoretical analysis based on structural data obtained from a sparkle model *J. Lumin.* **75** 255 68

[39] Binnemans K 2009 Lanthanide based luminescent hybrid materials *Chem. Rev.* **109** 4283 374

[40] Ishida H, Tobita S, Hasegawa Y, Katoh R and Nozaki K 2010 Recent advances in instrumentation for absolute emission quantum yield measurements *Coord. Chem. Rev.* **254** 2449 58

[41] Shavaleev N M, Pope S J A, Bell Z R, Faulkner S and Ward M D 2003 Visible light sensitisation of near infrared luminescence from Yb(iii) Nd(iii) and Er(iii) complexes of 3,6 bis(2 pyridyl)tetrazine *Dalton Trans.* **2003** 808 14

[42] Ilibi M, de Queiroz T B, Ren J, De Cola L, de Camargo A S S and Eckert H 2014 Luminescent hybrid materials based on covalent attachment of Eu(iii) tris (bipyridinedicarboxylate) in the mesoporous silica host MCM 41 *Dalton Trans.* **43** 8318

[43] Innocenzi P, Kozuka H and Yoko T 1997 Fluorescence properties of the Ru(bpy)32 + complex incorporated in sol gel derived silica coating films *J. Phys. Chem.* B **101** 2285 91

[44] Matsui K and Momose F 1997 Luminescence properties of Tris (2,2′ bipyridine)ruthenium(II) in sol gel systems of SiO$_2$ *Chem. Mater.* **9** 2588 91

[45] Sun L N, Zhang H J, Meng Q G, Liu F Y, Fu L S, Peng C Y, Yu J B, Zheng G L and Wang S B 2005 Near infrared luminescent hybrid materials doped with lanthanide (Ln) complexes (Ln = Nd, Yb) and their possible laser application *J. Phys. Chem.* B **109** 6174 82

[46] Feng J, Song S Y, Deng R P, Fan W Q and Zhang H J 2010 Novel multifunctional nanocomposites: magnetic mesoporous silica nanospheres covalently bonded with near infrared luminescent lanthanide complexes *Langmuir* **26** 3596 600

[47] Liu Y, Sun L, Liu J, Peng Y X, Ge X, Shi L and Huang W 2015 Multicolor (vis NIR) mesoporous silica nanospheres linked with lanthanide complexes using 2 (5 bromothiophen)imidazo[4, 5 f][1, 10] phenanthroline for *in vitro* bioimaging *Dalton Trans.* **44** 237 46